Chaos, Solitons and Fractals 113 (2018) 238–243

Contents lists available at ScienceDirect

Chaos, Solitons and Fractals

Nonlinear Science, and Nonequilibrium and Complex Phenomena

journal homepage: www.elsevier.com/locate/chaos

Review

Effects of a parametric perturbation in the Hassell mapping

Juliano A. de Oliveira[a,b,*], Hans M.J. de Mendonça[a], Diogo R. da Costa[a], Edson D. Leonel[a,c]

[a] Universidade Estadual Paulista (UNESP), Instituto de Geociências e Ciências Exatas, Departamento de Física, Câmpus de Rio Claro, Av.24A, 1515, SP 13506-900, Brazil

[b] Universidade Estadual Paulista (UNESP), Câmpus de São João da Boa Vista, Av. Profa. Isette Corrêa Fontão, 505, SP 13876-750, Brazil

[c] Abdus Salam International Center for Theoretical Physics, Strada Costiera 11, Trieste 34151, Italy

ARTICLE INFO

Article history:
Received 9 March 2018
Revised 14 May 2018
Accepted 12 June 2018
Available online 23 June 2018

MSC:
00-01
99-00

Keywords:
Perturbed Hassell mapping
Convergence to the stationary state
Extreming curves
Parameter space

ABSTRACT

The convergence to the fixed point near at a transcritical bifurcation and the organization of the extreming curves for a parametric perturbed Hassell mapping are investigated. The evolution of the orbits towards the fixed point at the transcritical bifurcation is described using a phenomenological approach with the support of scaling hypotheses and homogeneous function hence leading to a scaling law related with three critical exponents. Near the bifurcation the decay to the fixed point is exponential with a relaxation time given by a power law. The extreming curves in the parameter space dictates the organization for the windows of periodicity, consequently demonstrating how the set of shrimp-like structures are organized.

1. Introduction

Discrete time can be used to characterize the evolution of dynamical systems described by the so called mappings. Investigations might consider dissipative as well as non-dissipative dynamics in either 1-D or higher dimensions. The literature on iterated mappings is vast [1–6] and is always increasing. The studies on this sort of dynamical systems increased after the seminal papers of May and co-authors [7,8]. The dynamics reveals a complicated and intricate organization either as function of the control parameter or time [9,10], namely periodic orbits, bifurcations of different types including both local – transcritical, tangent, period doubling etc. – and global such as boundary crisis, merging attractor crisis, interior crisis, chaos and its different routes. The convergence to the fixed point at the bifurcation was proved to obey an homogeneous function characterized by a set of three critical exponents [11,12], while near the bifurcation the dynamics evolves to the stationary state via an exponential decay [13] whose relaxation time is characterized by a power law on the distance from the bifurcation. These four exponents define the class of universality of the bifurcation. After that the Hassell mapping [14,15] was considered to explore the evolution towards the equilibrium near the transcritical bifurcation [16].

In this paper we investigate the effects of a parametric perturbation in the dynamical properties of a Hassell mapping, with the main goal of to understand and describe the effects of the parametric perturbation in the convergence to the fixed point as well as to characterize the organization of the extreming curves in the parameter space [17,18]. The investigation to the asymptotic state will be made by using an homogeneous function [19]. The parameter space investigation shall allow us to understand the organization of the returning curves hence given the organization of the chaotic and periodic domains as a function of the control parameters [17].

This work is organized as follows: Section 2 describes the map, bifurcation diagram and the convergence to the fixed point. Section 3 is devoted to the analytical studies on the convergence to the fixed point at the transcritical bifurcation and in its neighboring. Section 4 is placed to discuss about the parameter space and the extreming curves. Finally, in Section 5 we present the discussions and conclusions.

2. The model

The model we consider is a time perturbed Hassell mapping written as

$$N_{n+1} = N_n\lambda(1 + b_n\epsilon)[1 + \alpha N_n]^{-\gamma}, \quad (1)$$

* Corresponding author at: Universidade Estadual Paulista (UNESP), Câmpus de São João da Boa Vista, Av. Profa. Isette Corrêa Fontão, 505, SP 13876-750, Brazil.
E-mail address: juliano.antonio@unesp.br (J.A. de Oliveira).

https://doi.org/10.1016/j.chaos.2018.06.017
0960-0779/

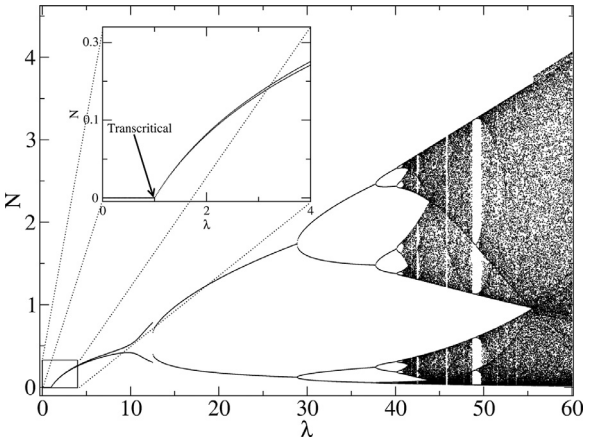

Fig. 1. Bifurcation diagram of the parametric perturbed Hassell mapping (1), using $\alpha = 1$, $\gamma = 6$, $\epsilon = 0.01$ and the initial condition $N_0 = 0.1$. The parameter λ was considered in the range $\lambda \in [0, 60]$.

where $\alpha > 0$, $\gamma > 0$ and $\lambda > 0$ are control parameters and ϵ controls the amplitude of the parametric perturbation, b_n is chosen as $b_n = (-1)^n$ or $b_n = (-1)^{n+1}$, so that for a given initial condition N_0 it can be set as $b_0 = 1$ or $b_0 = -1$. If $\epsilon = 0$ the Hassell mapping [14–16] is recovered. The time perturbation is periodic - period 2 -, it implies that, in order to find the fixed points and to study the convergence of the orbits to the stationary state, we have to calculate the map (1) in its 2th iteration, i.e., N_{n+2}. Rewriting $(n+2)$ and n in a convenient way, such that $(n+2) \to (m+1)$ and $n \to m$, we obtain

$$N_{m+1} = \lambda^2(1-\epsilon^2)N_m \times\left[(1+\alpha N_m) + \alpha\lambda(1-\epsilon)N_m(1+\alpha N_m)^{(-\gamma+1)}\right]^{-\gamma}. \quad (2)$$

Fig. 1 shows the bifurcation diagram of map (1) and we aim to investigate what happens to the behavior of the system at the fixed point $N^* = 0$ and at the transcritical bifurcation obtained from

$$\left(\frac{dN_{m+1}}{dN_m}\right)_{N_{m+1}=N^*} = 1, \quad (3)$$

yielding $\lambda_c = \frac{1}{\sqrt{(1-\epsilon^2)}}$, where the bifurcation arises (see zoom box in the Fig. 1).

To describe the convergence to the steady state we analyze the map from second iteration and looking the behavior of N approaching to the fixed point at the transcritical bifurcation. The convergence depends on the number of iterations n, on the initial condition N_0 and the parameter $\mu = \lambda_c - \lambda \cong 0$, which defines the distance from the bifurcation point. The parameter $\mu = 0$ establishes the transcritical bifurcation in the fixed point $N^* = 0$. In this way, the convergence is shown in Fig. 2 and we choose $\alpha = 1$, $\gamma = 6$, $\epsilon = 0.01$ and different initial conditions N_0 (as labeled in the figure). The procedure used can be made for another values of γ too.

A careful investigation of Fig. 2, allows us to see that different initial conditions lead to different curves with similar behaviors. They have a plateau at short n and a regime of power law decay for large enough n converging to the same fixed point. The changeover from the plateau to the decay is marked by a characteristic crossover iteration number n_x. From the behavior shown in that figure, we can suppose

1. For a short n typically $n \ll n_x$, the behavior of N_n *vs.* n is given by $N_n \propto N_0^{\alpha}$ leading to $\alpha = 1$;
2. For $n \gg n_x$, we notice $N_n \propto n^{\beta}$ where β is called a decay exponent;

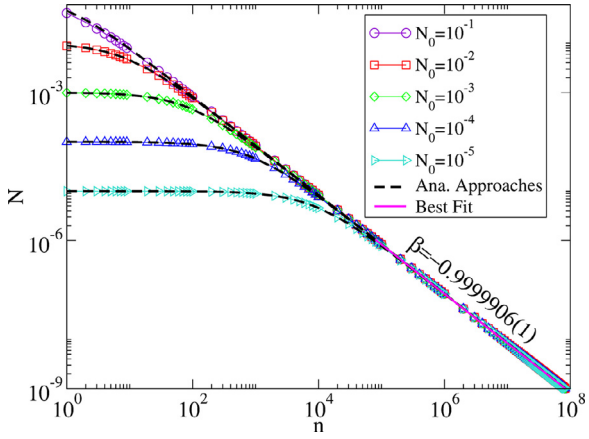

Fig. 2. Convergence to the fixed point $N^* = 0$ considering as fixed $\alpha = 1$, $\gamma = 6$, $\epsilon = 0.01$ and the different initial conditions shown in Fig. Here $\lambda_c = 1/\sqrt{(1-\epsilon^2)}$.

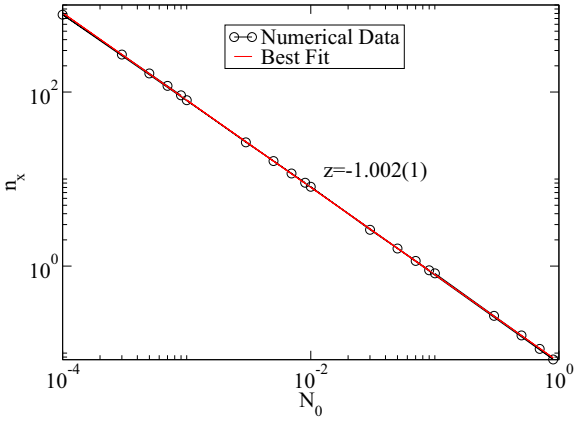

Fig. 3. Crossover iteration number n_x against the initial condition N_0, yielding through a power law fit $z = -1$.

3. Finally the crossover iteration number n_x is given by $n_x \propto N_0^z$, where z is a changeover exponent.

A power law fitting in the regime of decay in Fig. 2 gives $\beta = -0.999987(1)$. The exponent z is obtained from the plot of n_x *vs.* N_0, as shown in Fig. 3. Using $\alpha = 1$, $\gamma = 6$ and $\epsilon = 0.01$ we obtained through a power law fitting $z = -1$. The behavior shown in Fig. 2 together with the scaling hypotheses allow us to describe the behavior of N_n as homogeneous function of the variables n and N_0, when $\mu = 0$, of the type

$$N(N_0, n) = lN(l^{\tilde{a}}N_0, l^{\tilde{b}}n), \quad (4)$$

where l is a scale factor, $\tilde{a}$ and $\tilde{b}$ are characteristic exponents. Doing a similar procedure as made in Ref. [11] we obtain that

$$z = \frac{\alpha}{\beta}. \quad (5)$$

The knowledge of any two exponents allows us to find the third one by using Eq. (5). Moreover, the exponents can also be used to rescale the variables N_n and n in a convenient way, such that $N \to \frac{N}{N_0^{\alpha}}$ together with $n \to \frac{n}{N_0^z}$ to overlap all curves of N *vs.* n onto a single and hence universal curve, as shown in Fig. 4.

Let us now discuss the behavior of the convergence of the orbits to the fixed point not at the bifurcation, but rather close to it. This is the case when $\mu \neq 0$ and the decay is marked by an exponential law given by Hohenberg and Halperin [19], and Leonel et al. [20]

$$N(n, \mu) \propto e^{-n/\tau}, \quad (6)$$

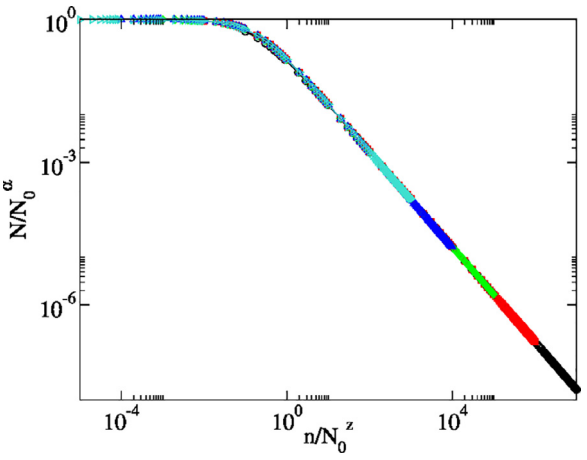

Fig. 4. Overlap of all curves shown in Fig. 2 onto a single and universal plot, after a convenient rescale of the axis.

where τ is the relaxation time given by

$$\tau \propto \mu^{\delta}, \tag{7}$$

here μ defines the relaxation parameter and the exponent δ gives the speed of the decay. From the simulations and fitting δ in a power law, we obtained $\delta = -1$.

3. Analytical approach

To have a better insight near the fixed point and as an attempt to describe the convergence of the orbits to the stationary state in a more robust way, it turns out to be convenient to expand the map (2) in its second iteration in Taylor series near the fixed point $N^* = 0$. Considering only the terms of lowest nonlinear contribution, we end up with

$$N_{m+1} = \lambda^2(1-\epsilon^2)N_m[1 - aN_m], \tag{8}$$

where $a = \gamma\alpha[1 + \lambda(1-\epsilon)]$. We suppose that close to the fixed point the dynamical variable N can be considered as a continuous variable. Then, for the case of $\mu = 0$, Eq. (8) is written as

$$\begin{aligned} N_{m+1} &= \lambda_c^2(1-\epsilon^2)N_m - \lambda_c^2(1-\epsilon^2)aN_m^2, \\ N_{m+1} - N_m &= \frac{N_{m+1} - N_m}{(m+1) - m}, \\ &\approx \frac{dN}{dm} = -aN^2. \end{aligned} \tag{9}$$

Grouping the terms properly we obtain the following first order differential equation

$$\frac{dN}{N^2} = -a\ dm. \tag{10}$$

The initial condition N_0 is defined by $m = 0$, while for variable m we have N_m. Applying these variables as integration limits, we have

$$\int_{N_0}^{N(m)} \frac{dN'}{N'^2} = -\int_0^m a\ dm'. \tag{11}$$

Proceeding with the integration and regrouping we have

$$N(m) = \frac{N_0}{[amN_0 + 1]}. \tag{12}$$

Let us then discuss the implications of Eq. (12) for specific values of m. We start with the case $amN_0 \ll 1$, which is equivalent to the first scaling hypotheses $n \ll n_x$. For such a case we obtain that $N(m) \propto N_0$ and allows us to conclude that $\alpha = 1$. Second we consider the situation $amN_0 \gg 1$, corresponding to $n \gg n_x$ in the second scaling hypotheses. For such case we obtain that

$$N(m) \propto m^{-1}. \tag{13}$$

Comparing this result with second scaling hypothesis, we conclude that $\beta = -1$. Finally when $amN_0 = 1$, which is the case of the third scaling hypotheses $n = n_x$, we obtain

$$n_x \propto N_0^{-1}, \tag{14}$$

therefore leading to $z = -1$. Using this procedure we obtained all the three exponents discussed in the previous section, being in a good agreement with the numerical results. The Fig. 2 show us the decay of the orbits to the fixed point N^*, with the analytical approaches indicated by the dashed lines. Those curves were obtained from Eq. (12).

We now study the behavior of the convergence to the fixed point when $\mu \neq 0$. The mapping is rewritten as

$$\begin{aligned} N_{m+1} - N_m &= \left(\frac{\lambda}{\lambda_c}\right)^2 N_m - N_m, \\ &= \frac{N_{m+1} - N_m}{(m+1) - m} \approx \frac{dN}{dm}, \\ &= -\mu\tilde{k}N_m, \end{aligned} \tag{15}$$

where $\mu = \lambda_c - \lambda$ and $\tilde{k} = (\frac{\lambda+\lambda_c}{\lambda_c^2})$. Considering again that for $m = 0$ the initial condition is N_0, we have to integrate the following equation

$$\int_{N_0}^{N(m)} \frac{dN'}{N'} = -\mu\tilde{k}\int_0^m dm', \tag{16}$$

which leads to

$$N(m) = N_0 e^{-\mu\tilde{k}m}. \tag{17}$$

Comparing this result with Eqs. (6) and (7), we conclude that the exponent $\delta = -1$ has the same decay speed to the fixed point like in [16].

4. Parameter space investigation

This section is devoted to investigate the parameter space. To do that we shall use Lypaunov exponents Λ to discriminate between chaos and regular dynamics. For the considered system, the Lyapunov exponent is obtained as

$$\Lambda = \lim_{n\to\infty} \frac{1}{n} \ln\left(\frac{\partial N_{n+1}}{\partial N_n}\right). \tag{18}$$

The dynamics is chaotic when Λ is positive while negative values define regularity, that might include periodic or quasi periodic orbits. Fig. 5(a)–(d) show the parameter space λ as a function of ϵ, considering mapping (1) for $\alpha = 1$ and $\gamma = 6$. The colors represent the Lyapunov exponent Λ in (a) and (c), while the period of the orbits is used in (b) and (d). To obtain Fig. 5(a) we chose 10^6 combinations of λ and ϵ. For each pair of control parameters we iterate the map for up to 10^6 iterations that is completely disregarded therefore being assumed as transient. After that the Lyapunov exponent Λ is calculated for the next 10^6 iterations. As shown in Fig. 5(a) periodic structures, called as shrimp structures [18], have negative values of Λ, marked as the orange to yellow pallet color. Positive Lyapunov represents the chaotic structures and change from green to blue. The periodic structures can be highlighted when plotting the period as shown in Fig. 5(b). One can notice the existence of a pattern of distribution of these structures, where the extreming curves are the responsible for this distribution. The understanding of them allows one to predict where the periodic

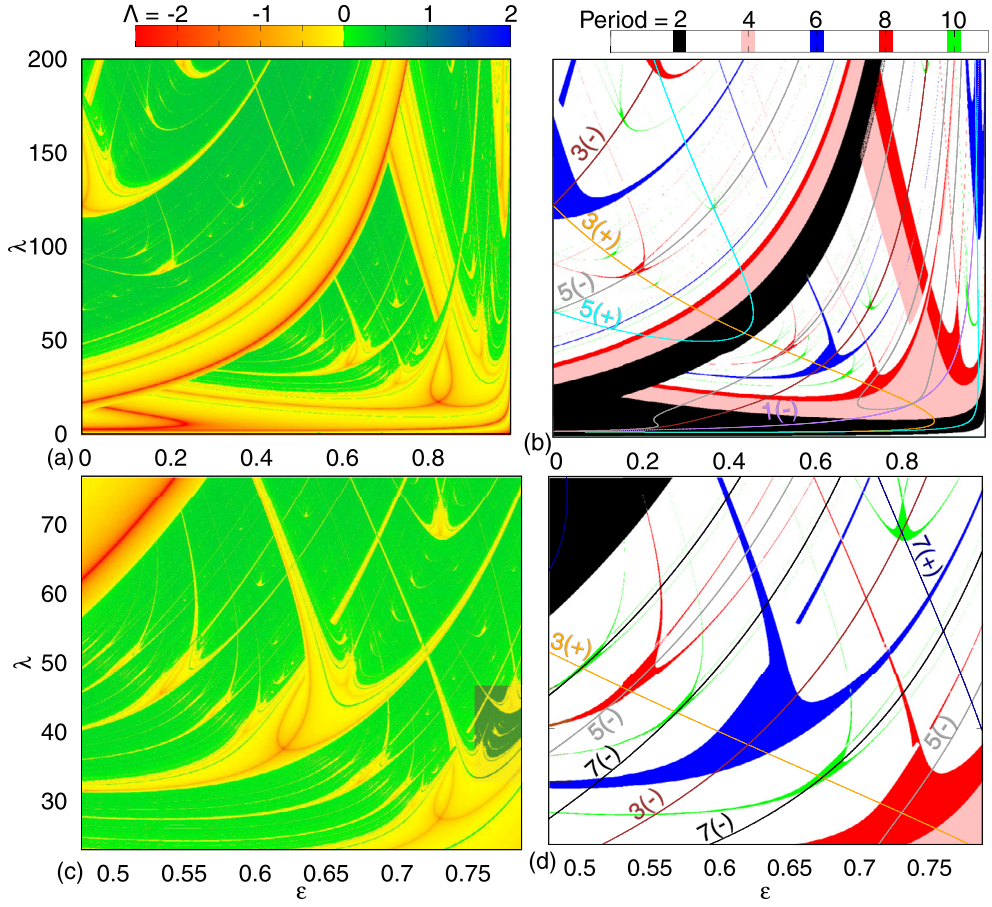

Fig. 5. The parameter space for the mapping (1) is shown. In (a) and (c) the color represents the Lyapunov exponent Λ, while in (b) and (d) the period is highlighted.

orbits exist in a parameter space. da Costa et al. [17] shows some details of these ones for the perturbed logistic map as well as the circle map.

To find the superstable orbits and also the extreming curves, it is important to calculate the conditions that lead to $\Lambda \to -\infty$, and it happens when

$$\frac{\partial N_{n+1}}{\partial N_n} = 0. \tag{19}$$

This equation contains, at least, one of the solutions $\{\tilde{N}_1, \tilde{N}_2, \ldots, \tilde{N}_i, \ldots, \tilde{N}_j, \ldots\}$ and in the first iterate it has as solution

$$\tilde{N} = \frac{1}{\alpha(\gamma - 1)}. \tag{20}$$

An extreming curve is an orbit given by

$$\tilde{N}_i = F^{(k)}(\tilde{N}_j), \tag{21}$$

where $\tilde{N}_i$ and $\tilde{N}_j$ are solutions of Eq. (19), that also contain $\tilde{N}$, as one of the iterations of the mapping. For the system considered here, one can obtain the first extreming curve considering $N_{n+1} = N_n = \tilde{N} = \frac{1}{\alpha(\gamma-1)}$, which leads to

$$\epsilon = \frac{1}{b_n}\left[\frac{\left(1+\alpha\tilde{N}\right)^{\gamma}}{\lambda} - 1\right]. \tag{22}$$

It is important to remember that b_n assumes two different values -1 and $+1$, and the extreming curve with period 1 and $b_n = -1$ is represented in Fig. 5(b) as the curve $1(-)$.

When we consider

$$N_{n+2} = N_n = \tilde{N}, \tag{23}$$

a superstable curve with period 2 is obtained. Considering

$$u = \lambda(1-\epsilon) \quad \text{and} \quad v = \lambda(1+\epsilon), \tag{24}$$

yields immediately that

$$u + v = 2\lambda \quad \text{and} \quad u - v = -2\lambda\epsilon. \tag{25}$$

Solution of Eq. (23) gives

$$v = \frac{1}{u\left\{(1+\alpha N_n) + \alpha u N_n (1+\alpha N_n)^{(1-\gamma)}\right\}^{-\gamma}}. \tag{26}$$

So, to obtain the superstable orbit with period 2 one needs to vary u in order to obtain v and after that one can find the values of ϵ and λ through Eq. (25).

A extreming curve with period 3 can also be obtained. For this it is necessary to solve $N_{n+3} = N_n = \tilde{N}$. To find this solution it is convenient to define

$$z = (1+\alpha N_n) + u\alpha N_n (1+\alpha N_n)^{(1-\gamma)}, \tag{27}$$

and

$$q = uvN_n z^{-\gamma}. \tag{28}$$

Therefore, we find

$$u = \frac{N_n}{q[1+\alpha q]^{-\gamma}}, \tag{29}$$

and

$$v = \frac{q}{uN_n\left[(1+\alpha N_n) + u\alpha N_n (1+\alpha N_n)^{(1-\gamma)}\right]^{-\gamma}}. \tag{30}$$

The main idea is to vary the value of q to find u through Eq. (29). After that one finds the value of v in Eq. (30). With these values we

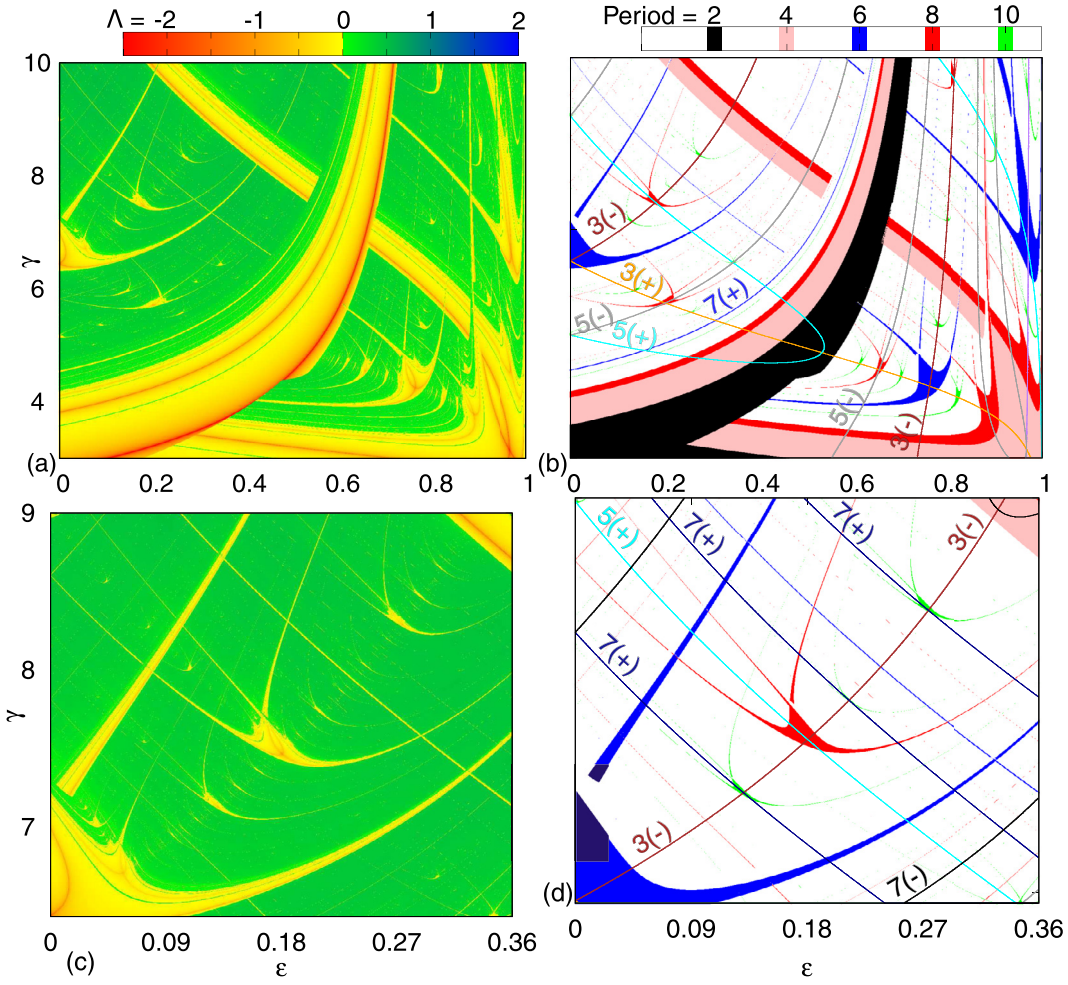

Fig. 6. The parameter space for the mapping (1) is shown. In (a) and (c) the color represents the Lyapunov exponent Λ, while in (b) and (d) the period is highlighted.

obtain the values of λ and ϵ using Eq. (25). The extreming curves with period 3 are shown in Fig. 5(b) and (d) as $3(+)$ and $3(-)$. These ones dictates the organization of many periodic structures of the parameter space. Therefore, they play an important role for a dissipative system. The other high order extreming curves were obtained numerically, for example, making $N_{n+5} = N_n = \tilde{N}$ highlights the extreming curves with period 5 (represented as $5(+)$ and $5(-)$). When two of these curves with different signs intercept each other, we have that the period of a shrimp is the sum of the period of each extreming curve. As an illustration, observe the curves $5(-)$ and $3(+)$ in Fig. 5(b). When they intercept each other a shrimp of period 8 (represented as the red color) appears.

If two extreming curves with same sign intercept each other, the period of the shrimp is given by subtracting the period of these curves. The intercept of the curve $5(+)$ and $3(+)$ in Fig. 5(b) happens at the same location of a period 2 shrimp ($|5-3| = 2$).

Fig. 6(a)–(d) show the parameter space γ as function of ϵ for $\alpha = 1$ and $\lambda = 100$. In Fig. 6(a) we have a plot of the periodic structures, where in Fig. 6(b) the colors show the period of these ones, while the colored curves represent the extreming curves obtained analytically and numerically. Fig. 6(c) shows an enlargement in Fig. 6(a), where another cascade of shrimps can be observed in details.

5. Discussions and conclusions

We have studied decay to the fixed point at the transcritical bifurcation in the time perturbed Hassell mapping and the organization of the extreming curves in the parameter space. The convergence leads to a set of three critical exponents at the bifurcation, namely $\alpha = 1$, $\beta = -1$ and $z = -1$, therefore the same universality class of the bifurcation observed in the logistic map and in the original Hassell map. In fact, the periodic perturbation did not affect the critical exponents obtained in the Hassell map. The relevant relation of the critical exponent is summarized in the scaling law $z = \alpha/\beta$. Near the bifurcation the convergence is exponential and with a relaxation time given by $\tau \propto \mu^{\delta}$ with $\delta = -1$. The parameter space was investigated by the use of both Lyapunov exponents and period of the orbits. The extreming curves dictate the organization for the windows of periodicity. We have shown how to obtain these orbits for this mapping both numerically and analytically.

Acknowledgments

JAO thanks CNPq (421254/2016-5), (311105/2015-7) and FAPESP (2014/18672-8)(Brazilian agencies). HMJM acknowledges FAPESP (2015/22062-3)(Brazilian agency). DRC acknowledges PNPd/CAPES (Brazilian agency). EDL thanks to CNPq (303707/2015-1), FUNDUNESP and FAPESP (2017/14414-2, 2012/23688-5, 2008/57528-9, 2005/56253-8)(Brazilian agencies). This research was supported by resources supplied by the Center for Scientific Computing (NCC/GridUNESP) of the São Paulo State University (UNESP).

References

[1] Hilborn RC. Chaos and nonlinear dynamics: an introduction for scientists and engineers. New York: Oxford University Press; 1994.
[2] Zang WB. Discrete dynamical systems, bifurcations and chaos in economics. Elsevier Science; 2006.
[3] Martelli M. Introduction to discrete dynamical systems and chaos. New York: Wiley; 1999.
[4] Devaney RL. A first course in chaotic dynamical systems: theory and experiment (studies in nonlinearity). Cambridge: Westview Press; 1992.
[5] Galor O. Discrete dynamical systems. Heildelberg: Springer; 2007.
[6] Devaney RL. An introduction to chaotic dynamical systems. Cambridge: Westview Press; 2003.
[7] May RM. Science 1974;86:645.
[8] May RM, Oster GA. Am Nat 1976;110:573.
[9] Luo ACJ, O'Connor DM. System dynamics with interaction discontinuity (nonlinear systems and complexity). Springer; 2015.
[10] Ott E. Chaos in dynamical systems. Cambridge: Cambridge University Press; 2002.
[11] Teixeira RMN, Rando DS, Geraldo FC, Costa Filho RN, de Oliveira JA, Leonel ED. Phys Lett A 2015;379:1246.
[12] Leonel ED, Teixeira RMN, Rando DS, Costa Filho RN, de Oliveira JA. Phys Lett A 2015;379:1796.
[13] Hirsch JE, Huberman BA, Scalapino DJ. Phys Rev A 1982;25:519.
[14] Hassell MP. J Anim Ecol 1975;44:283.
[15] Panik MJ. Growth curve modeling: theory and applications. Wiley; 2013.
[16] de Mendonça HMJ, Leonel ED, de Oliveira JA. Physica A 2017;466:537.
[17] da Costa DR, Hansen M, Guarise G, Medrano-T RO, Leonel ED. Phys Lett A 2016;380:1610.
[18] Gallas JAC. Phys Rev Lett 1993;70:2714.
[19] Hohenberg PC, Halperin BI. Rev Mod Phys 1977;49:435.
[20] Leonel ED, da Silva JKL, Kamphorst SO. Int J Bifurc Chaos 2002;12:1667.